

## **Electronic Supplementary Information (ESI)**

### **Vermiculite as a natural silicate crystal for hydrogen generation from photocatalytic splitting of water under visible light**

Jian Zhang, Tianyu Liu, Rui Chen, and Xiaoheng Liu

Key Laboratory for Soft Chemistry and Functional Materials of Ministry of Education, Key Laboratory of Jiangsu Province for Chemical Pollution Control and Resources Reuse, Nanjing University of Science and Technology, Nanjing, 210094, P.R. China. \**E-mail: xhliu@mail.njust.edu.cn*

## 1. Experimental details

### 1.1 Sample preparation

All the reagents used in this work, including  $\text{H}_2\text{PtCl}_6$  and ethylene glycol were of AR grade from the Shanghai Chemical Factory of China and were used without further purification. In a typical synthesis of Pt/VMT nanocomposites, 0.10g VMT (pure VMT, from Weili of Xinjiang Province in China) was dispersed in ethylene glycol (20 ml) and stirred for a few minutes. Then the weight ratios of  $\text{H}_2\text{PtCl}_6 \cdot 6\text{H}_2\text{O}$  to VMT were 0, 1.0%, 3.0%, and 5.0%, and the obtained samples were labeled as Pt0, Pt1, Pt3, and Pt5, respectively. After keeping stirring for 15 min, the homogeneous solution was transferred into a Teflon-lined autoclave of 50 ml capacity (180 °C for 12 h). The final products were washed with ethanol several times.

### 1.2 Sample characterization

Transmission electron microscopy (TEM) images and energy dispersive X-ray (EDX, EDAX Genesis 2000) spectroscopy were performed on a JEOL JEM-2100 microscope operating at 200 kV. Field-emission scanning electron microscopy (FESEM) was performed with a LEO1550 microscope. VMT was characterized by XRD on a Bruker D8 Advance X-ray powder diffractometer with Cu K $\alpha$  radiation ( $\lambda=1.5418 \text{ \AA}$ ). UV-Vis absorption spectra were obtained using a Ruili UV-1201 spectrophotometer. The chemical composition of VMT was estimated using a inductively coupled spectrometry (ICP) (Optima 5300DV). Valence band X-ray photoelectron spectra (XPS) were acquired on an ESCALAB 250 with Al K $\alpha$  ( $h\nu=1486.6 \text{ eV}$ ) as the excitation source.

### 1.3 Photocatalytic activity test

Typically, reactions were carried out in a closed gas-circulation system. A 300 W Xenon lamp (XL-300, Yirida Co. Ltd.) was used as the light source, and visible light irradiation was realized by attaching a 450 nm cutoff filter. 0.1 g catalyst was dispersed in an aqueous solution (200 ml) containing triethanolamine (TEOA) (5%, v/v) as the sacrificial electron donor and Eosin Y (0.0555 g) as photosensitizer. The system was evacuated several times prior to irradiation. The evolved hydrogen was analyzed by an online gas chromatography (GC-1690, Jiedao, TCD, Ar carrier).

The apparent quantum efficiency (QE) was measured under the same photocatalytic reaction condition. A model 1916-R Newport power meter was used for the intensity measurement of light. The QE plotted were estimated by using several cut-off filters, and were calculated on the basis of the number of the incident photons in each wavelength region. Accordingly, each value is plotted in the middle of two cut-off wavelengths. The QE was calculated according to eq (1):

$$\begin{aligned} \text{QE}[\%] &= \frac{\text{number of reacted electrons}}{\text{number of incident photons}} \times 100 \\ &= \frac{\text{number of evolved H}_2 \text{ molecules} \times 2}{\text{number of incident photons}} \times 100 \end{aligned} \quad (1)$$

### 1.4 Fabrication of photoanodes of VMT

The working electrodes were prepared as follows. 5 mg of VMT was suspended in 1 ml ethanol under ultrasonic treatment to make slurry. The slurry was then coated onto a 2.0 cm×1.0 cm F-doped SnO<sub>2</sub>-coated glass electrode by the doctor blade method. Next, the resulting electrodes were dried in an oven and calcined at 200 °C for 30 min. The photoelectrochemical properties were investigated in a conventional

three-electrode cell using an electrochemical analyzer (CHI-610B, Shanghai Chenhua, China) and the prepared samples as the working electrodes, a Pt wire as the counter electrode, and Ag/AgCl (saturated KCl) as a reference electrode. The light source was a 300W Xe lamp. The light intensity was tuned to  $200 \text{ mW cm}^{-1}$  and 1 M NaOH aqueous solution was used as the electrolyte and the bias sweep range was from 0.4 to 1.0 V with the step size of 5 mV. The samples were illuminated from the back side and the front side, respectively. The potentials of the working electrodes can be calculated using the formula  $V_{\text{RHE}} = V_{\text{Ag/AgCl}} + 0.059\text{pH} + 0.1976\text{V}$ , where  $V_{\text{RHE}}$  is a potential vs. a reversible hydrogen potential,  $V_{\text{Ag/AgCl}}$  is a potential vs. Ag/AgCl electrode, and pH is the pH value of electrolyte.

**Table S1.** Comparison of the QE for hydrogen evolution.

Reference	Photocatalyst	Photosensitizer	Incident light	QE (%)
<b>This work</b>	<b>3 wt% Pt/VMT</b>	<b>Eosin Y</b>	<b>&gt;450 nm</b>	<b>22.8 (at 483 nm)</b>
Ref. 1	1 wt% Pt/TiO <sub>2</sub> via Fe <sup>3+</sup> coupling	Eosin Y	>420 nm	19.1 (>420 nm)
Ref. 2	1 wt% Pt, Ru, Rh/ Ti-MCM-41 Zeolite	Eosin Y	>420 nm	12 (>420 nm)
Ref. 3	7 wt% Pt/Reduced graphene oxide	Eosin Y	>420 nm	4.2 (>420nm)
Ref. 4	TiO <sub>2</sub>	Zinc-substituted cytochrome	>475 nm	10
Ref. 5	3.0 wt% Pt/TiO <sub>2</sub>	Ru-complex	>420 nm	22.4
Ref. 6	0.1wt% Pt/K <sub>4</sub> Nb <sub>6</sub> O <sub>17</sub>	Ru(bpy) <sub>3</sub> <sup>2+</sup>	>420 nm	22 (at 450 nm)
Ref. 7	Co(dmgh) <sub>2</sub> (py)Cl	Eosin Y	>450 nm	4 (at 530 nm)
Ref. 8	7% Pt/g-C <sub>3</sub> N <sub>4</sub>	Eosin Y	>420 nm	18.8 (>420 nm)

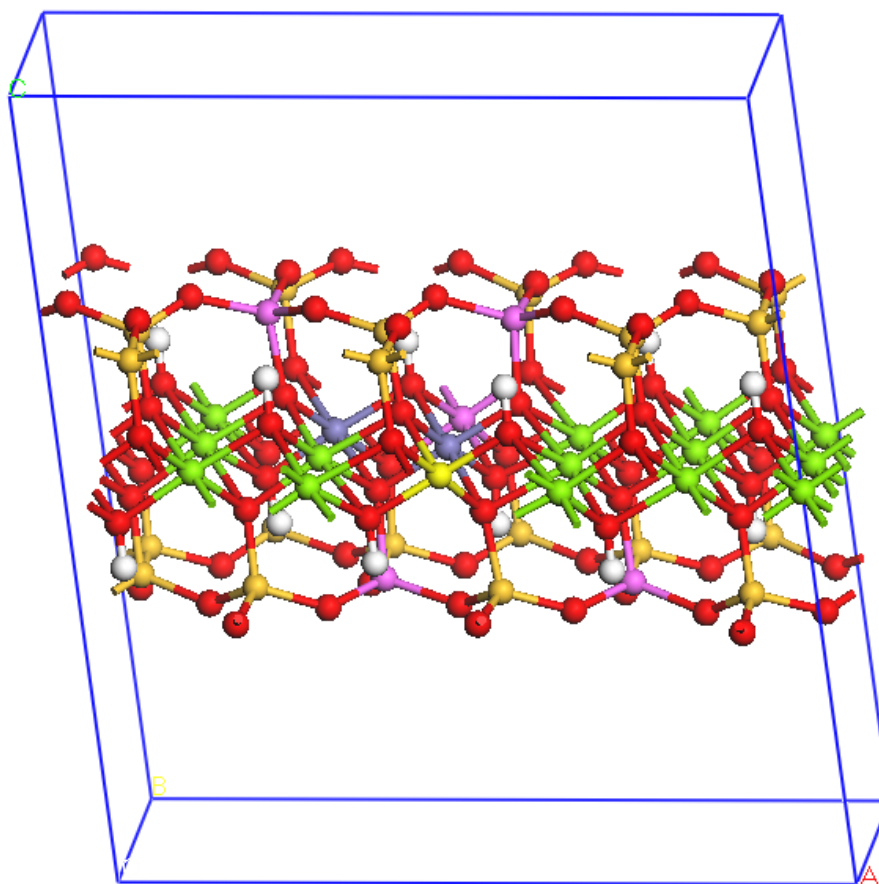


**Figure S1.** The proposed structure of VMT. Atoms: red balls-O, green balls-Mg, white balls-H, yellow balls-Si, purple balls-Al, blue balls-Fe.

By using VASP code,<sup>9</sup> structures have been optimized and the ion-electron interaction is described with the projected augmented wave (PAW)<sup>10,11</sup> method and the exchange-correlation functional is PW91<sup>12</sup> based on the generalized gradient approximation (GGA) and the convergence threshold was set to  $10^{-5}$  eV in energy and 0.02 eV/Å in force.

Optimal structure of VMT used in our work was determined through three steps:

Firstly, there are five kinds of possible structures when two Fe doping in one super cell (Figure S2). The energy corresponding to Figure S2 is shown in Table S2.

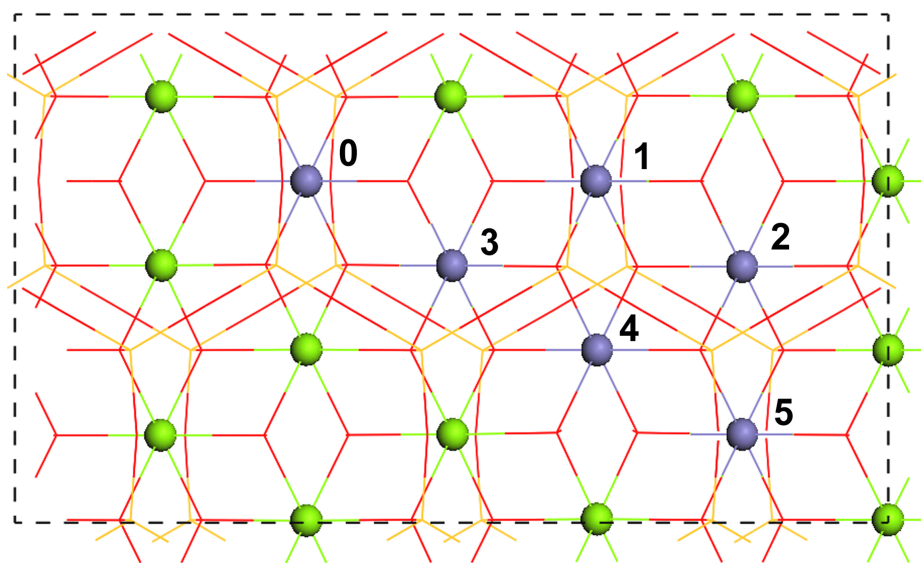


**Figure S2.** Five kinds of possible structures when two Fe doping in one super crystal cell. Fixed one Fe as 0, five kinds of possible structures were sited 1, 2, 3, 4, 5, respectively. Atoms: red crosses-O, green balls-Mg, yellow crosses-Si, blue balls-Fe.

**Table S2.** The summary of the energy corresponding to Figure S2.

verm-Fe-sites-1	-891.751577 eV
verm-Fe-sites-2	-891.748050 eV
verm-Fe-sites-3	<b>-891.752685 eV</b>
verm-Fe-sites-4	-891.748089 eV
verm-Fe-sites-5	-891.732288 eV

Secondly, there are six kinds of possible structures when one Al doping in one super cell (Figure S3). The energy corresponding to Figure S3 is shown in Table S3.

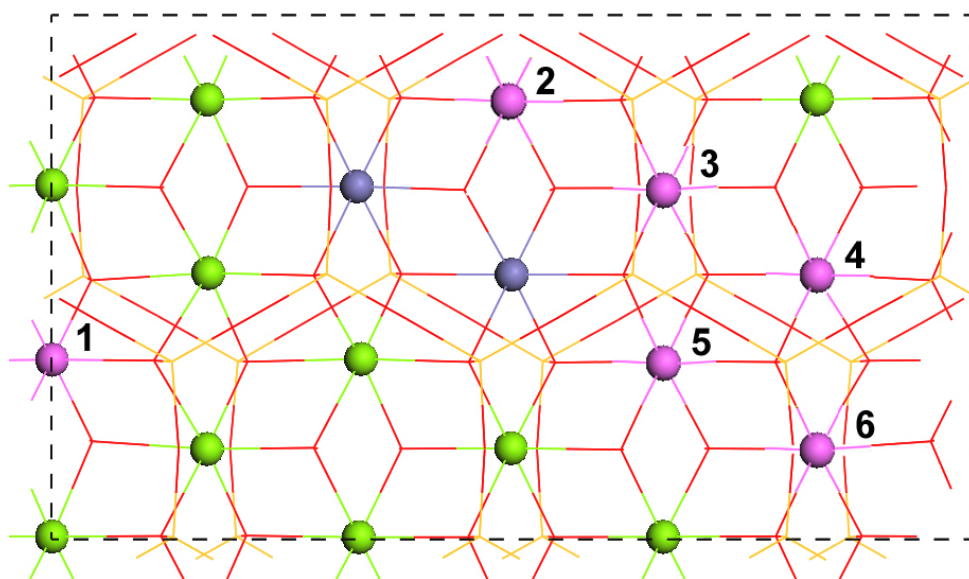
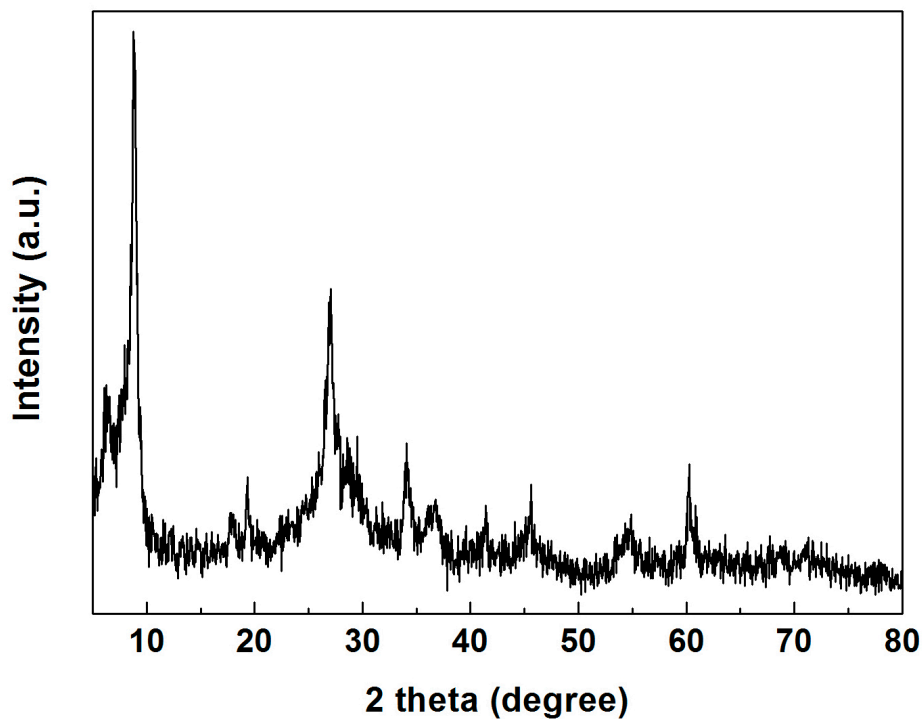


**Figure S3.** Six kinds of possible structures when one Al doping in one super crystal cell. Six kinds of possible structures were sited 1, 2, 3, 4, 5, respectively. Atoms: red crosses-O, green balls-Mg, yellow crosses-Si, blue balls-Fe, purple balls-Al.

**Table S3.** The summary of the energy corresponding to Figure S3.

1Al-site-in-2Fe-1	-891.621216
1Al-site-in-2Fe-2	<b>-891.855802</b>
1Al-site-in-2Fe-3	-891.765994
1Al-site-in-2Fe-4	-891.629205
1Al-site-in-2Fe-5	-891.781833
1Al-site-in-2Fe-6	-891.624161

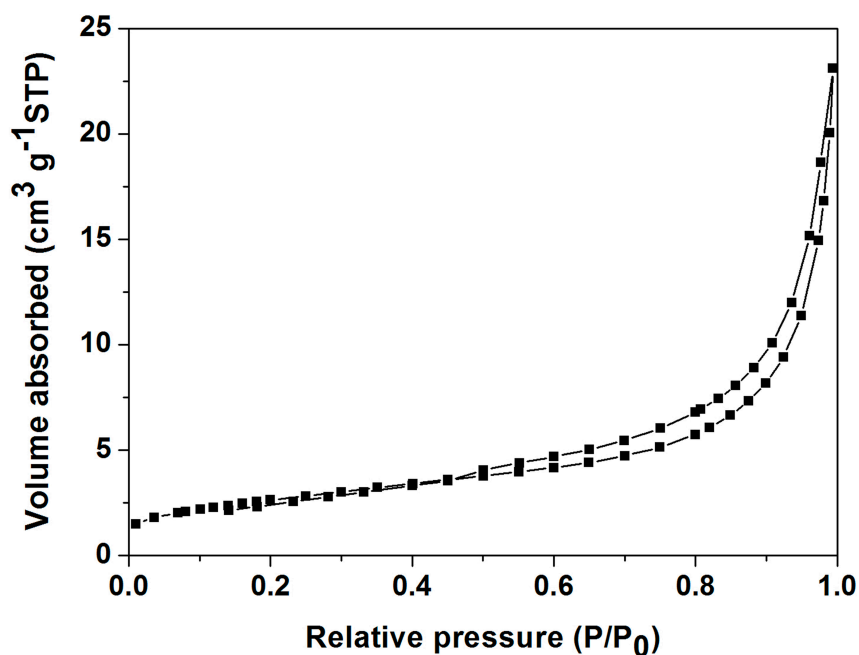
Finally, the sites of the rest of Al were determined through the same method. The final structure we proposed is shown in Figure S1.



**Figure S4.** XRD pattern of VMT.

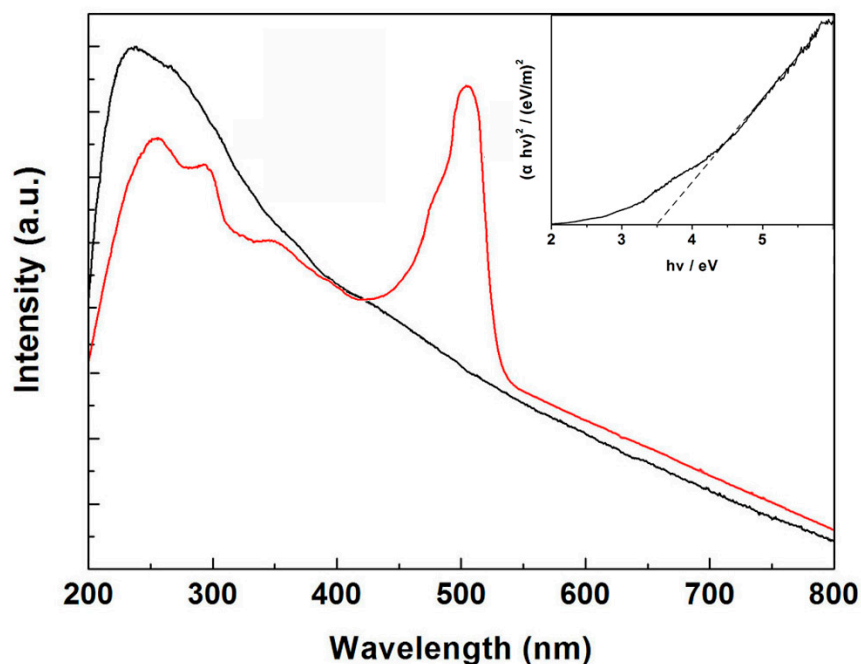
Figure S4 shows the XRD pattern of the VMT. There are two peaks in the low-angle region. The weak but sharp peak at  $2\theta = 6.2^\circ$  probably corresponds to packets of VMT platelets. The intense broad band at  $2\theta = 7.5^\circ$  is interpreted as the interstratification of the VMT platelets. We can not find structure information of standard VMT in Bruker XRD database, but it is quite similar to previous report.<sup>13</sup>





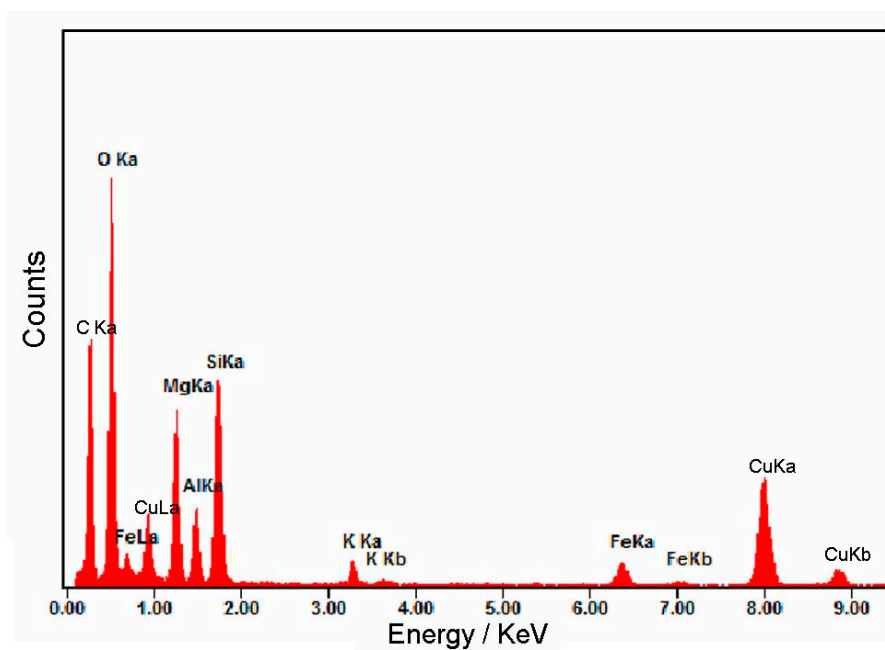
**Figure S5.** Nitrogen adsorption-desorption isotherms of VMT.

Figure S5 shows the  $N_2$  adsorption-desorption isotherms of VMT. The VMT clay exhibits a  $N_2$  isotherm close to type IV (in the IUPAC classification) with one clear H3-type hysteresis loop from  $P/P_0 = 0.46$  to 1.00 owing to narrow slit-shaped pores.<sup>14</sup> In addition, the specific surface area ( $9.88 \text{ m}^2 \text{ g}^{-1}$ ) corresponding to external surface area without any microporosity. The low surface area is related to the surface charge of the particle. The strong hydrogen bonds between the tetrahedral sheet and the water of interlayer cations in VMT can keep the interlayer zone obstructed, which could reduce superficial nitrogen adsorption considerably.<sup>15</sup>



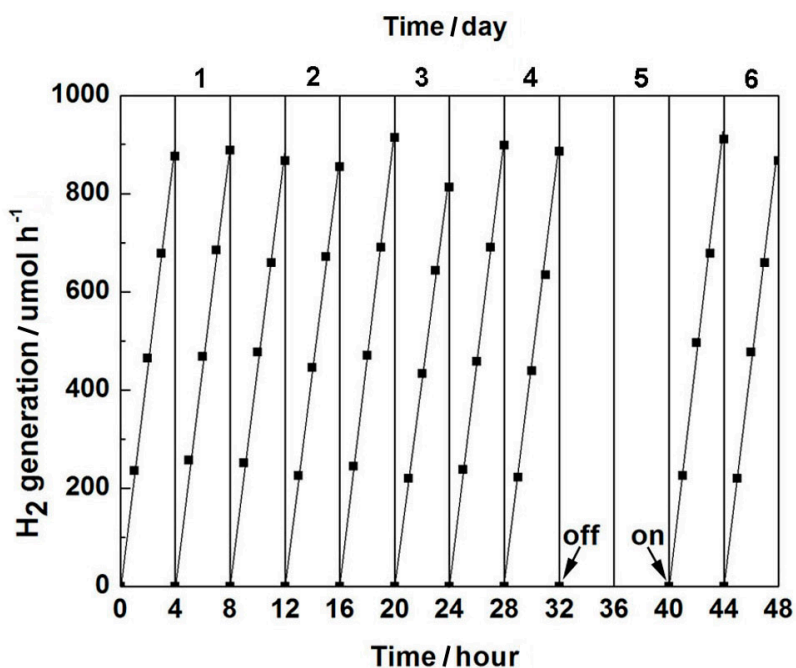
**Figure S6.** UV-Vis absorption spectra of VMT with (red curve) and without EY (black curve).

Figure S6 shows UV-Vis absorption spectra of VMT and EY adsorbed to VMT. The UV-Vis absorption spectrum in Figure S6 (black curve) shows strong semiconductor-like absorption in the UV region as well as intrinsic and wide absorption in visible region. In order to enhance visible light photocatalytic ability, some organic dyes as visible light irradiation sensitizers have attracted great attention for water splitting. The UV-Vis absorption spectrum in Figure S6 (red curve) shows EY adsorbed to VMT. However, comparing with UV-Vis absorption spectrum of VMT (black curve), the absorption at visible wavelengths steeply increases in the wavelength of 450-550 nm, in which the main adsorption band of EY.<sup>16</sup>



**Figure S7.** TEM-EDX elemental analysis of VMT

The result of EDX elemental analysis for pure VMT is displayed in Figure S7. The elements C and Cu are from sample supporter of TEM observation, and other elements including O, Si, Mg, Al, K and Fe are all from VMT. Remarkably, Figure S7 confirms existence of Fe, and its content is closed to ICP measurement (4.7 %) within the error of EDX.  $K^+$  distributed in the interlayer of VMT.



**Figure S8.** Cycling measurement of hydrogen generation through direct photocatalytic water splitting with VMT under visible light.

The VMT sample can exhibit substantial activity and stability in the photocatalytic production of hydrogen from water under visible light. Hydrogen evolution as a function of time during a 6-day testing period of visible light driven hydrogen production experiment using VMT as the photocatalyst is shown in Figure S6. The hydrogen produced was evacuated every 4 h in successive runs. Measurement was conducted for 6 consecutive days; each day the sample was irradiated for 8 hours and then stored in darkness overnight before testing the next day. Continuous hydrogen evolution with no noticeable degradation of the VMT was clearly observed from the beginning of the reaction. After testing for 4 days, the sample was stored in darkness for 1 day without measurement. Experiment was resumed for 1 more day after the 1-day storage period, and similar rates of hydrogen evolution was still observed. The total evolution of hydrogen after 40 h was 8775  $\mu\text{mol}$  ( $219 \mu\text{mol h}^{-1}$ , average).

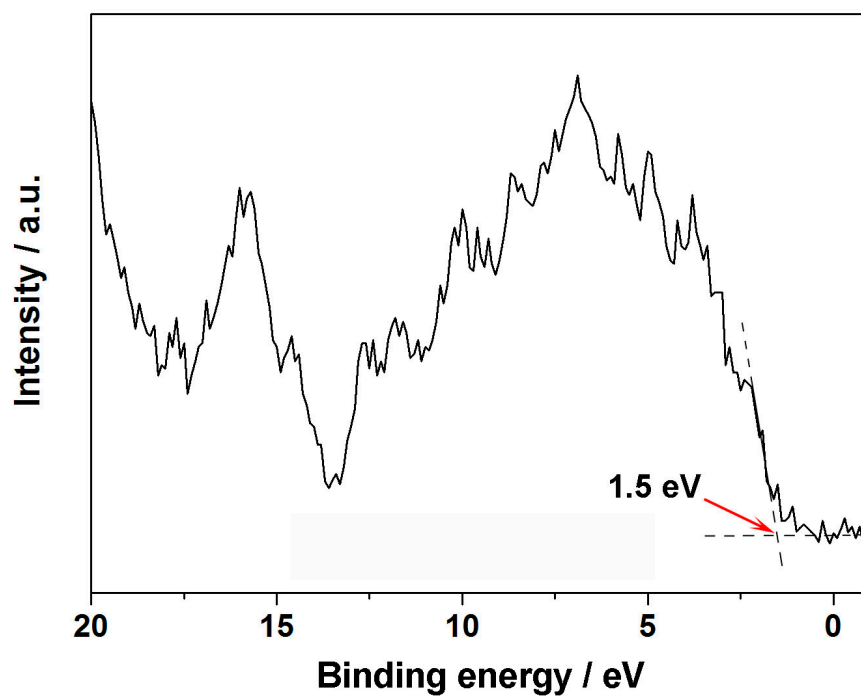


**Figure S9.** Valence band XPS spectra of the VMT.

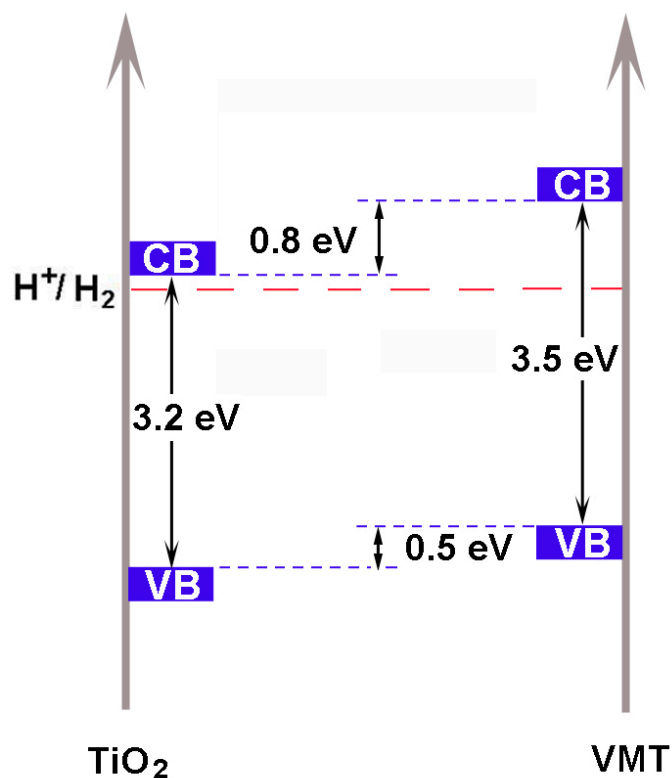


**Figure S10.** Electronic potential diagram for anatase TiO<sub>2</sub> and VMT.

## References

- 1 Y. X. Li, M. M. Guo, S. Q. Peng, G. X. Lu and S. B. Li, *Int. J. Hydrogen Energy*, 2009, **34**, 5629.
- 2 Q. Y. Li, Z. L. Jin, Z. G. Peng, Y. X. Li, S. B. Li and G. X. Lu, *J. Phys. Chem. C*, 2007, **111**, 8237.
- 3 S. X. Min and G. X. Lu, *J. Phys. Chem. C*, 2011, **115**, 13938.
- 4 Y. Astuti, E. Palomares, S.A. Haque and J. R. Durrant, *J. Am. Chem. Soc.*, 127, **2005**, 15120.
- 5 E. Bae and W. Choi, *J. Phys. Chem. B*, 2006, **110**, 14792.
- 6 K. Maeda, M. Eguchi, W. J. Youngblood and T. E. Mallouk, *Chem. Mater.*, 2009,

- 21**, 3611.
- 7 T. Lazarides, T. McCormick, P. Du, G. Luo, B. Lindley and R. Eisenberg, *J. Am. Chem. Soc.*, 2009, **131**, 9192.
- 8 J. Xu, Y. Li, S. Peng, G. Lu and S. Li, *Phys. Chem. Chem. Phys.*, 2013, **15**, 7657.
- 9 G. Kresse and J. Hafner, *Phys. Rev. B*, 1993, **47**, 558.
- 10 P. E. Blöchl, *Phys. Rev. B.*, 1994, **50**, 17953.
- 11 G. kresse and D. Joubert, *Phys. Rev. B.*, 1999, **59**, 1758.
- 12 J. P. Perdew and Y. Wang, *Phys. Rev. B.*, 1992, **45**, 13244.
- 13 T. Kogure, K. Morimoto, K. Tamura, H. Sato and A. Yamagishi, *Chem. Lett.*, 2012, **41**, 380.
- 14 K. S. W. Sing, D. H. Everett, R. A. W. Haul, L. Moscou, R. A. Pierotti, J. Rouquerol and T. Siemieniewska , *Pure Appl. Chem.*, 1985, **57**, 603.
- 15 D. Tunega, *Phys. Chem. Miner.*, 2003, **30**, 517.
- 16 X. Chen, S. Shen, L. Guo and S. S. Mao, *Chem. Rev.*, 2010, **110**, 6503.